Organic & Biomolecular Chemistry

ROYAL SOCIETY OF CHEMISTRY

PAPER

View Article Online
View Journal | View Issue

Cite this: *Org. Biomol. Chem.*, 2024, **22**, 4987

Bisindole-based small molecules as transmembrane anion transporters and potential anticancer agents†

Swati Bansi Salunke, [a] Shreyada N. Save, [b] Naveen J. Roy, [a] Ronedy Naorem, [a] Shilpy Sharma [b] and Pinaki Talukdar *[a]

Received 5th April 2024,
Accepted 27th May 2024

DOI: 10.1039/d4ob00554f

rsc.li/obc

Few synthetic ion transporters have been reported incorporating indole as the core moiety. We have developed a novel bisindole-based transporter capable of efficient transmembrane anion antiport. This system induced cytotoxicity in MCF-7 breast cancer cells *via* chloride ion homeostasis disruption and the associated ROS generation, mitochondrial membrane depolarization, and lysosomal deacidification.

Introduction

The transport of ions across the cell envelope is facilitated by various membrane-embedded proteins that aid the polar ion in overcoming the hydrophobic barrier of the lipid membrane.[1] This tightly regulated transport process, also known as ion homeostasis, is central to vital cellular processes.[1–3] It is possible to disrupt this delicate ion balance using small molecules that mimic these protein functions, either as ion carriers or channels, and initiate unregulated transmembrane ion transport. Such systems find application in the killing of diseased and cancerous cells.[4] Reports in recent literature show synthetic chloride ion transporters to be capable of inducing cancer cell death through the apoptotic pathway *via* perturbation of cellular chloride ion concentrations,[5–8] making the design of such small molecules to be of interest in supramolecular chemistry.

Prodigiosins are a well-known family of naturally occurring tripyrrolic transporters capable of transmembrane chloride transport[9,10] that show promising anticancer, antimicrobial, and antifungal properties.[11,12] The anticancer activity of prodigiosin is linked to its ion transport ability, where it can destabilize the ion homeostasis and induce apoptotic cell death.[13] Pyrrole with its hydrogen bond donor N–H forms the core of this system and has thus inspired the development of many pyrrole-based transporters including tambjamines,[14,15] calixpyrroles.[16,17] and amidopyrroles.[18,19] Like pyrrole, indole also has a single NH H-bond donor capable of anion binding, but surprisingly has been less studied as an anion transporter, even though indole NH is more acidic than pyrrole NH (pK_a in DMSO: pyrrole 23.0 and indole 21.0).[20] Until 2004, indole anion complexation was only recognized in biological systems as a binding core in the form of tryptophan in the nitrate,[21] sulfate,[22] and bicarbonate[23] binding proteins, and in haloalkane dehalogenase.[24] The first indole-based anion receptor was a macrocycle reported by Jeong and co-workers in 2005,[25] following which many more were reported by Gale and co-workers that included simple indole/biindole,[26] acyclic indole,[27] 2-amidoindole,[28] and 2,7-functionalized indole[29] moieties. Thenceforth, ion transporters having an indole core were pioneered by this group, who have reported drug-like properties of indole-substituted urea and thiourea-based anion transporters[30] and fused the pyrrole and imine part of prodigiosin with indole to develop perenosins.[31] These along with the indole amide system from our lab[32] are the only known reports of indole-based transporters, making indole less explored (relative to pyrrole) in the field of artificial ion transport.

Herein, we have designed and synthesized a series of substituted bisindole-based anionophores (**1a–1d**) by the coupling of indole-2-carboxylic acid with ester derivatives of 7-aminoindole-2-carboxylic acid. Tuning of the transporter log*P* value was achieved by variation of the chain length of alkyl groups attached to the ester moiety (Fig. 1). From the predicted N–H group pK_a values (MarvinSketch),[33] 11.92 for (indole) N–H_a, 15.88 for (amide) N–H_b, and 10.45 for (indole) N–H_c (Fig. 1), we hypothesized the bisindole system could effectively complex with an anion through hydrogen bonding with its three N–H groups and transport the anion across the membrane, while the indole rings efficiently shielded the charge from the hydrophobic environment of the lipid bilayer.

[a]*Department of Chemistry, Indian Institute of Science Education and Research (IISER) Pune, Dr. Homi Bhabha Road, Pashan, Pune 411008, Maharashtra, India. E-mail: ptalukdar@iiserpune.ac.in*

[b]*Department of Biotechnology, Savitribai Phule Pune University (Formerly University of Pune), Pune 411007, Maharashtra, India*

†Electronic supplementary information (ESI) available: Details of synthetic protocols and characterization of compounds, crystallographic parameters, experimental protocols, including vesicle preparation, ion transport assays and biological studies, additional data for ion transport studies, details of geometry optimized structures and additional biological data. CCDC 2306377. For ESI and crystallographic data in CIF or other electronic format see DOI: **https://doi.org/10.1039/d4ob00554f**

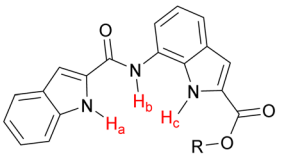

Compound	R	log*P*
1a	Ethyl	3.46
1b	Butyl	4.43
1c	Hexyl	5.32
1d	Octyl	6.21

pK_a values: NH_a: 11.92; NH_b: 15.88; NH_c: 10.45

Fig. 1 Structure of bisindole transporters with predicted NH pK_a and log*P* values.

Results and discussion

Synthesis

7-Nitroindole-2-carboxylic acid (**2**) was synthesized from *ortho*-nitroaniline according to the known literature procedure.[34] Ester derivatives **3a–3d** were synthesized by the coupling of acid **2** with different aliphatic alcohols in the presence of EDC·HCl and DMAP (Scheme 1). The corresponding amines **4a–4d** were obtained by the reduction of the nitro group of **3a–3d** using H_2, Pd/C. Finally, coupling of amines **4a–4d** with indole-2-carboxylic chloride yielded the desired anionophores **1a–1d**. Prediction of log*P* of derivatives with calculator plugins of MarvinSketch yielded values close to 5 (Fig. 1), which ensured good lipid membrane permeability in line with Lipinski's rule, making them suitable for transmembrane ion transport.

Amid all synthesized compounds **1a–1d**, the crystal for **1d** was obtained by slow evaporation of solvent from the saturated solution of **1d** in DMSO. The transporter was found to co-crystallize with DMSO, where the amide N–H_b and indole N–H_c interacted with the oxygen atom of the solvent through hydrogen bonds, while indole N–H_a formed H-bond with the amide carbonyl group of the neighboring bisindole molecule, contributing to the 3D crystal packing (Fig. S15†).

Ion transport studies

The ion transport properties of compound **1a–1d** were investigated across 8-hydroxypyrene-1,3,6-trisulfonate (HPTS) dye entrapped large unilamellar vesicles (LUVs), prepared from egg-yolk phosphatidylcholine (EYPC) (EYPC–LUVs ⊃ HPTS) (Fig. S1†) suspended in NaCl (100 mM)–HEPES (10 mM) buffer (pH = 7.0).[5] A pH gradient (pH_{in} = 7.0, pH_{out} = 7.8) was applied

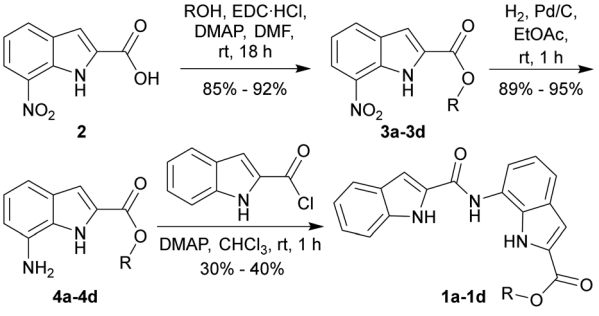

Scheme 1 Synthesis of the bisindole-based ion carriers **1a–1d**.

across the membrane by addition of NaOH following which the transporters (**1a–1d**) were added. The resultant ion transport induced dissipation of the pH gradient by **1a–1d** was measured by monitoring the time-based fluorescence intensity of HPTS at 450 nm (λ_{em} = 510 nm). Comparison of ion transport activities of **1a–1d** offered the activity sequence **1b** > **1c** ≈ **1a** > **1d** at 500 nM (0.80 mol%) concentration (Fig. 2A). Dose-dependent ion transport studies of **1a–1c** (Fig. S2–S4†) were conducted across EYPC–LUVs ⊃ HPTS and the EC_{50} values and Hill coefficients (n) of the transporters were obtained by fitting to the Hill equation (eqn (S2)†). The Hill plot analysis of most active transporter **1b** furnished EC_{50} = 347 nM (0.55 mol%) and the Hill coefficient, n = 1.3 suggesting only one molecule of **1b** interacts with an anion for active transporter complex formation. The calculated EC_{50} values for **1a** and **1c** were 751 nM (1.20 mol%) and 748 nM (1.19 mol%), and Hill coefficients 1.78 and 1.51, respectively. Hill analysis could not be performed for **1d** due to its precipitation at higher concentrations in the buffer.

Since transporter **1b** furnished the highest ion transport activity, mechanistic studies were conducted using this derivative. Variation of the extravesicular anion (Cl^-, Br^-, I^-, NO_3^-, ClO_4^-, and OAc^-) in EYPC–LUVs ⊃ HPTS (Fig. S5†) resulted in significant changes in the transport activity profile of **1b** (0.6 μM, 0.96 mol%) (Fig. 2B), indicating the process to be anion dependent. The dual gradient of pH and dissimilar anions created across the vesicular membrane in this assay can act in opposite directions, depending on the nature of the anion. In the case of the extravesicular I^-, NO_3^-, and ClO_4^-, which are hydrophobic anions, the ease of anion dehydration,[35] coupled with the higher hydrophobicity of the resulting transporter-anion complex allows for higher membrane permeability[36] and, thus, faster rates of ion transport compared to the corresponding chloride complex. Thus, in the case of I^-, NO_3^-, and ClO_4^-, the anion gradient dominates the initial phase of the transport process, leading to an influx of A^- balanced, at least in part, by OH^- efflux following transporter addition. This leads to an initial decrease in HPTS fluorescence as a consequence of the drop in intravesicular pH. The subsequent enhancement of the pH gradient eventually allows it to dominate the transport process, leading to OH^- influx balanced by Cl^- efflux which results in the increase of intravesicular pH and thus the dye fluorescence. This is not observed for the hydrophilic anions (Cl^-, Br^-, and OAc^-), where the pH gradient solely dictates the direction of anion transport.

As the ion transport process was anion dependent, the transporter induced Cl^- influx of **1a–1d** were evaluated across LUVs entrapped with lucigenin (EYPC–LUVs ⊃ lucigenin), across which a Cl^- gradient was generated (Fig. S6†). The Cl^- transport process was monitored from the change in fluorescence intensity of lucigenin at λ_{em} = 535 nm (λ_{ex} = 455 nm). Comparative studies showed the same order of transport activity as observed in HPTS assay, *i.e.*, **1b** > **1c** ≈ **1a** > **1d** (Fig. 2C). Dose-dependent studies of **1a** and **1b** across EYPC–LUVs ⊃ lucigenin followed by Hill analysis (Fig. S7 and S8†) yielded n = 2.05 (EC_{50} = 1.91 μM, 2.04 mol%) for **1a**, while

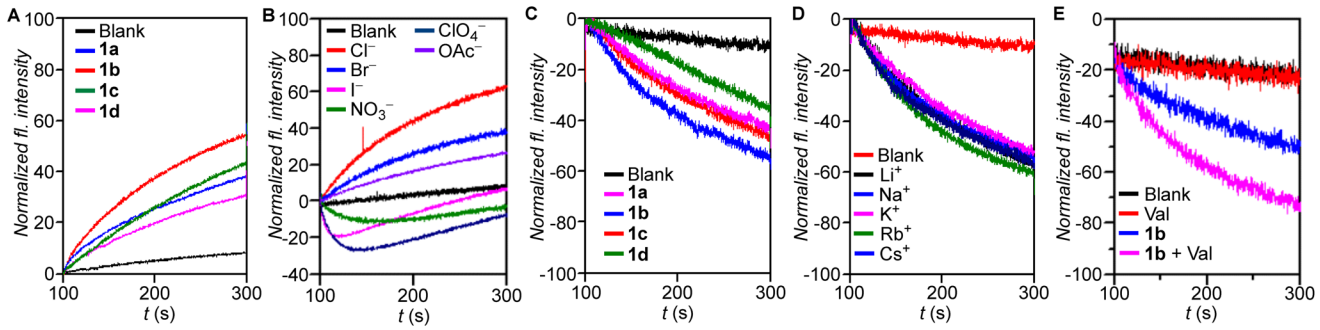

Fig. 2 (A) Comparison of ion transport activity of bisindole derivatives **1a–1d** (0.5 μM) and (B) anion selectivity assay of **1b** (0.6 μM) across EYPC–LUVs ⊃ HPTS. (C) Comparison of activities of **1a–1d** (2.5 μM), (D) cation selectivity assay of **1b** (2.5 μM) and (E) valinomycin (Val, 0.2 μM) coupled assay of **1b** (1 μM) across EYPC–LUVs ⊃ lucigenin.

n = 1.34 (EC_{50} = 1.24 μM, 1.32 mol%) was obtained for **1b** which agreed with data from the HPTS assay. Hill analysis could not be performed for compounds **1c** and **1d** due to precipitation at higher concentrations. No change in the rate of transport of **1b** was observed on variation of extravesicular cations (Li^+, Na^+, K^+, Rb^+, and Cs^+) across EYPC–LUVs ⊃ lucigenin revealing the absence of cation transport (Fig. 2D). This indicated the transport process to be cation independent, suggesting either H^+/Cl^- symport or Cl^-/X^- antiport. Hence, the Cl^- transport properties of **1b** were evaluated in the presence and absence of the K^+ selective transporter valinomycin (Fig. S8†).[19] A significant increase in the ion transport activity of **1b** across EYPC–LUVs ⊃ lucigenin was observed following valinomycin treatment (Fig. 2E), confirming anion antiport as the mechanism of transport in bisindoles. The dual K^+, Cl^- gradient generated across the membrane at the start of the assay triggers unidirectional transport/influx of K^+ by valinomycin. The resulting charge gradient was neutralized by the Cl^- transport (influx) by the bisindole, resulting in a synergistic effect that aids both transport processes. Since net charge neutrality is maintained in this coupled transport process the reverse movement (efflux) of the NO_3^- by the transporter becomes redundant. Overall, a significant increase in the rate of Cl^- influx would be observed, leading to faster quenching of the lucigenin fluorescence if the mechanism of transport is anion antiport. For a symporter, no change in transport activity would be observed as the net transfer of charge is zero and is not influenced by the K^+ gradient.

Compounds **1a** and **1b** were tested for carrier mechanism of transmembrane ion transport through a variable temperature assay across 1,2-dipalmitoyl-*sn-glycero*-3-phosphocholine (DPPC) liposomes entrapping HPTS dye (DPPC–LUVs ⊃ HPTS) (Fig. S11†).[37] DPPC undergoes gel to liquid-crystalline phase transition at T_c = 41.3 °C.[38] The transport ability of both **1a** and **1b** (2.5 μM, 3.64 mol%) were inhibited at 25 °C, when lipid was in gel phase, which then recovered above T_c at 45 °C (Fig. S12†). This confirmed the mobile carrier mechanism of ion transport, as carrier mobility is greatly inhibited in the gel phase.[37] Transport through ion channels are unaffected by the lipid phase due to their membrane spanning nature and thus this mechanism of ion transport can be ruled out for the bisindole system.

Hill analysis data indicated the formation of a 1 : 1 ($n \approx 1$, [**1b** + Cl^-]) transmembrane ion transport complex for transporter **1b** while **1a** formed a 2 : 1 ($n \approx 2$, [(**1a**)$_2$ + Cl^-]) complex, the theoretical prediction of whose structures were attempted. An initial prediction of the most probable geometry of [**1b** + Cl^-] complex using the CONFLEX 8 conformation search software package[39,40] using MMFF94S (2010-12-04HG) force field with a search limit of 10 kcal mol^{-1} yielded 101 conformers. Conformers with a predicted Boltzmann population <5% were discarded, leaving 7 conformers whose Density Functional Theory (DFT) geometry optimization was conducted on the Gaussian 09 program suite[41] using the B3LYP exchange–correlation functional[42,43] and 6-31G (d,p) basis set.[44,45] The resultant outputs were highly similar and the conformer with the lowest Hartree–Fock (HF) energy was chosen, which showed all three N–H groups to be involved in anion binding (Fig. 3A and S20†), as per our initial hypothesis. The binding energy was calculated to be −38.69 kcal mol^{-1}.

A similar conformation search for [(**1a**)$_2$ + Cl^-] complex yielded 10 726 predictions of which 6 conformers having Boltzmann population ≥ 5% were chosen and the rest were rejected. DFT geometry optimization (B3LYP/6-31G(d,p)) of the

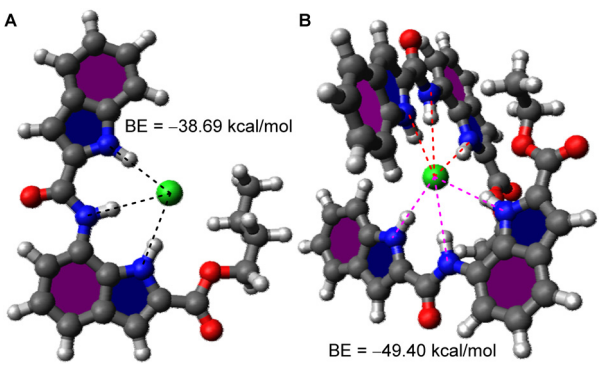

Fig. 3 Geometry optimized structures of ion transport complexes (A) [**1b** + Cl^-] and (B) [(**1a**)$_2$ + Cl^-] along with their calculated binding energies.

chosen conformers yielded highly similar structures of which the conformer with lowest HF energy was chosen. The resultant [(**1a**)$_2$ + Cl$^-$] complex showed two molecules of **1a** orthogonal to each other binding to Cl$^-$ (Fig. 3B, S18†) with all N–H groups participating in binding. The binding energy was calculated to be −49.40 kcal mol^{-1}.

For further verification of this interesting variation in ion complex formation in **1a** and **1b**, co-crystallization of the transporters with chloride ion (using tetrabutylammonium chloride (TBACl) as the Cl$^-$ source) was attempted in various solvent systems but ultimately unsuccessful. Hence, ^{1}H NMR ion titration studies were conducted with **1a** and **1b** in a 1 : 9 CD_3COCD_3/CD_3CN solvent system using TBACl as the chloride source (Fig. S13 and S14†). Downfield shifts were observed for all three NH peaks ((indole) N–H$_a$, (amide) N–H$_b$, and (indole) N–H$_c$) thereby confirming their participation in anion binding. The data was fitted to host–guest binding models using the BindFit program.[46] Data for transporter **1a** yielded a 2 : 1 transporter-ion binding stoichiometry with $K_{a1:1}$ = 137.7 M^{-1} ± 8.8% and $K_{a2:1}$ = 5862.7 M^{-1} ± 6.7%, while **1b** yielded a 1 : 1 stoichiometry with $K_{a1:1}$ = 2489.5 M^{-1} ± 3.7%, both of which were in agreement with data obtained from ion transport experiments, thereby validating our theoretical models. The large value of $K_{a2:1}$ for transporter **1a** indicated a strong preference for the formation of 2 : 1 transporter-ion complex over a 1 : 1 complex. Fitting of the data to the converse binding stoichiometries were tested, *i.e.*, 1 : 1 for transporter **1a** and 2 : 1 for **1b**, but these models yielded large error values for the fit and were thus rejected.

Biological studies

The promising results obtained from ion transport studies conducted for the bisindoles **1a–1d** encouraged us to assess their activities in biological systems. Initially, cell viability was assessed in the presence of **1a–1d** using MTT assay in non-cancerous mouse embryonic fibroblasts (MEFs) and MCF-7 breast cancer cells. While significant cytotoxicity was observed in MCF-7 cells following incubation with **1a–1d** for 24 h (Fig. 4A); negligible cytotoxicity was observed in the non-cancerous MEFs (Fig. 4B). This indicated of some level of selectivity of our bisindole system in the MCF-7 cancerous cells at the concentrations tested. Amongst the different derivatives tested, transporter **1a** was found to be most potent in terms of its anti-cancerous activity, although highest ion transport activity was observed for **1b**. The discrepancy in the results obtained could likely be attributed to the difference in membrane composition between the mammalian cells and the artificial liposomes used in the study. An IC_{50} value of 15 μM was obtained for **1a** in MCF-7 cells.

To further evaluate whether the cytotoxicity mediated by **1a** was dependent on Cl$^-$ transport, an MTT assay was performed in the presence and absence of Cl$^-$ ion in the extracellular media. In line with our previous observations, cytotoxicity was observed in MCF-7 cells grown in extracellular media containing Cl$^-$ ions when compared to cells cultured in extracellular media without Cl$^-$ ions upon exposure to **1a** (Fig. 4C). These results confirmed the importance of extracellular Cl$^-$ ions for

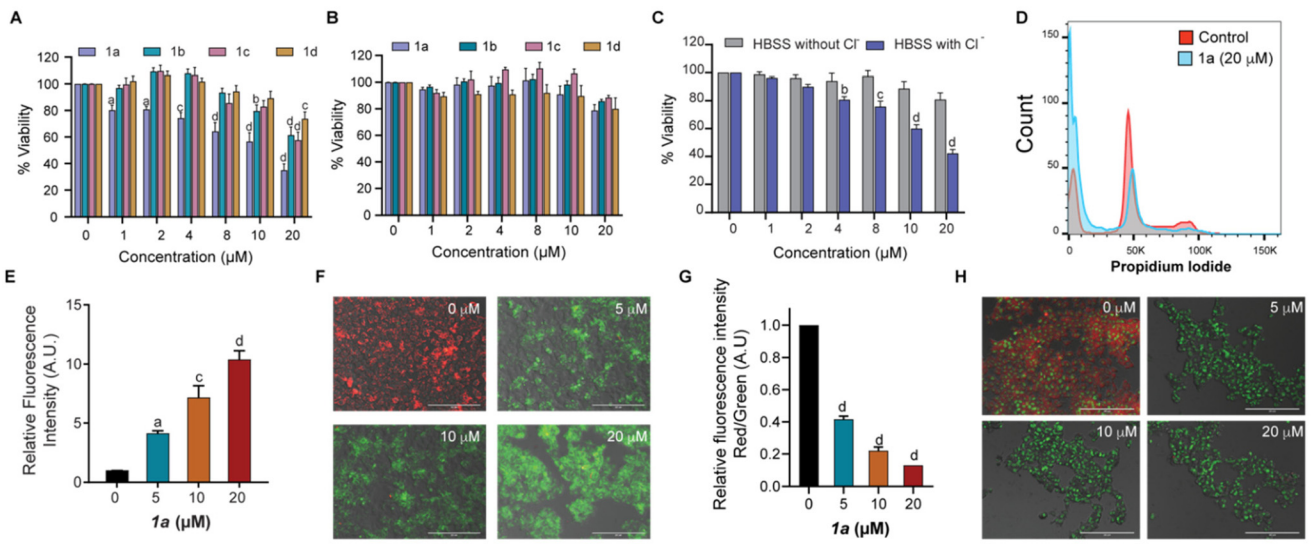

Fig. 4 Biological studies evaluating the anticancer potential of the bisindole compounds **1a–1d**. Cellular viability of the (A) MCF-7 breast cancer cells and (B) noncancerous MEFs, on treatment with **1a–1d** as assessed by MTT assay. The untreated wells were set at 100% viability and the relative viability for the different compounds has been depicted. (C) Cellular viability of **1a** in MCF-7 cells in the presence of HBSS with and without chloride ions. (D) Representative cell cycle profile of MCF-7 cells exposed to 20 μM concentration of **1a** (cyan) *versus* control cells (red). (E) Assessment of mitochondrial ROS levels using the MitoSox Red assay. (F) Representative images of JC-1 stained MCF-7 cells after treatment with increasing concentrations of **1a** (0, 5, 10 and 20 μM); and (G) quantitation of the changes in the MMP (expressed as the changes in red/green ratio) with increasing concentrations of **1a**. (H) Live cell images of MCF-7 cells stained with acridine orange upon treatment with increasing concentrations of **1a** (0, 5, 10 and 20 μM). Magnification 20×. Scale bar: 200 μm. a represents $p < 0.05$; b represents $p < 0.01$; c represents for $p < 0.001$; and d for $p < 0.0001$, when compared to untreated control using Tukey HSD tests.

bisindole-mediated toxicity observed in MCF-7 cells, thereby indicating transporter-mediated chloride transport to be the initiator of cell death.[8,47] This was associated with altered cell cycle profiles with reduced percentage of cells observed in the G1 and S/G2M phases with a significant increase in the G0 population in **1a** treated MCF-7 cells (Fig. 4D and S21D†). To further evaluate the presence of oxidative stress, mitochondrial ROS levels in MCF-7 cells were quantified using the probe MitoSOX Red, a compound known to rapidly oxidize to a highly fluorescent product in the presence of ROS. Increasing dosage of **1a** (0–20 μM) in MCF-7 yielded higher readout of MitoSOX fluorescence, thereby confirming the generation of ROS species (Fig. 4E). Increased ROS levels lead to alteration of mitochondrial membrane potential (MMP), a hallmark of cells experiencing cell death through the intrinsic apoptotic pathway. Next, we investigated the possibility of mitochondrial membrane depolarization using MMP-sensitive JC-1 dye, which forms red fluorescent J-aggregates in healthy mitochondria. Loss of MMP results in release of dye molecules into the cytoplasmic medium, which gives green intracellular fluorescence. Following treatment of MCF-7 cells with **1a** (0–20 μM) for 24 h, a decrease in red fluorescence of the JC-1 dye along with a subsequent increase in green fluorescence was observed on imaging under fluorescence microscope (Fig. 4F), indicating mitochondrial membrane depolarization as a result of bisindole facilitated disruption of chloride ion homeostasis. The quantification of red/green fluorescence showed an increase in MMP depolarization with increasing concentrations of **1a** (Fig. 4G). The depolarization of MMP causes an interruption in the electron transport chain of the mitochondrial respiratory cycle, leading to the generation of reactive oxygen species (ROS). In addition to this, an increase in the lysosomal pH (measured by acridine orange staining) was observed in cells exposed to **1a**. As the concentration of **1a** was increased, a decrease in red fluorescence with a concomitant increase in green fluorescence was observed, thereby indicating towards increase in the lysosomal pH (Fig. 4H). Thus, it can be concluded that **1a** mediates cytotoxicity in MCF-7 cells by disruption of chloride ion homeostasis, which is associated with increased oxidative stress, mitochondrial membrane depolarization and lysosomal pH disruption.

Conclusions

In summary, we have demonstrated the bisindole system to be an efficient transmembrane anion antiporter capable of inducing cytotoxicity in MCF-7 breast cancer cells *via* destabilization of cellular chloride ion homeostasis. Tuning of the ion transport property was achieved through variation of alkyl chain length of the substituted ester group. This perturbation of the cellular ion homeostasis by the bisindole transporter resulted in mitochondrial membrane depolarization, enhanced ROS generation and alteration in lysosomal pH in MCF-7 cells.

Author contributions

S. B. S. and P. T. designed the project and established research plans. S. B. S. synthesized and characterized compounds, and conducted chemical studies. S. N. S. conducted biological studies under the supervision of S. S. N. J. R. performed the computational studies. R. N. and N. J. R. characterized some compounds, performed some vesicle assays and ion titration studies. N. J. R., S. B. S. and S. N. S. wrote the manuscript. P. T. and S. S. revised the manuscript. All authors have given approval to the final version of the manuscript.

Conflicts of interest

There are no conflicts to declare.

Acknowledgements

P. T. acknowledges the financial support of the Science and Engineering Research Board, Government of India (Grant No. CRG/2022/001640) and IISER Pune. S. S. acknowledges funding from University Grants Commission, Government of India (Grant No. F.4-5(18-FRP) (IV-Cycle)/2017(BSR)) and RUSA 2.0 to SPPU. S. B. S. thanks DST, India for the Inspire Fellowship. S. N. S. has been supported by Mahatma Jyotiba Phule Research Fellowship, Government of Maharashtra (Mahajyoti/Nag./Fellowship/2021-22/1042 (418)). N. J. R. acknowledges the Council of Scientific & Industrial Research (CSIR), Government of India, for research fellowship. This research used the resources of the PARAM Brahma supercomputing facility at IISER Pune.

References

1 D. C. Gadsby, *Nat. Rev. Mol. Cell Biol.*, 2009, **10**, 344.
2 S. Y. Chiu and G. F. Wilson, *J. Physiol.*, 1989, **408**, 199–222.
3 K. Lange, *J. Cell. Physiol.*, 2000, **185**, 21–35.
4 P. A. Gale, J. T. Davis and R. Quesada, *Chem. Soc. Rev.*, 2017, **46**, 2497–2519.
5 T. Saha, M. S. Hossain, D. Saha, M. Lahiri and P. Talukdar, *J. Am. Chem. Soc.*, 2016, **138**, 7558–7567.
6 N. Busschaert, S.-H. Park, K.-H. Baek, Y. P. Choi, J. Park, E. N. W. Howe, J. R. Hiscock, L. E. Karagiannidis, I. Marques, V. Félix, W. Namkung, J. L. Sessler, P. A. Gale and I. Shin, *Nat. Chem.*, 2017, **9**, 667.
7 N. J. Roy, S. N. Save, V. K. Sharma, B. Abraham, A. Kuttanamkuzhi, S. Sharma, M. Lahiri and P. Talukdar, *Chem. – Eur. J.*, 2023, **29**, e202301412.
8 S.-K. Ko, S. K. Kim, A. Share, V. M. Lynch, J. Park, W. Namkung, W. Van Rossom, N. Busschaert, P. A. Gale, J. L. Sessler and I. Shin, *Nat. Chem.*, 2014, **6**, 885.
9 H. Konno, H. Matsuya, M. Okamoto, T. Sato, Y. Tanaka, K. Yokoyama, T. Kataoka, K. Nagai, H. H. Wasserman and S. Ohkuma, *J. Biochem.*, 1998, **124**, 547–556.

10 A. Fürstner, *Angew. Chem., Int. Ed.*, 2003, **42**, 3582–3603.
11 G. A. Islan, B. Rodenak-Kladniew, N. Noacco, N. Duran and G. R. Castro, *Bioengineered*, 2022, **13**, 14227–14258.
12 N. Darshan and H. K. Manonmani, *J. Food Sci. Technol.*, 2015, **52**, 5393–5407.
13 J. L. Sessler, L. R. Eller, W.-S. Cho, S. Nicolaou, A. Aguilar, J. T. Lee, V. M. Lynch and D. J. Magda, *Angew. Chem., Int. Ed.*, 2005, **44**, 5989–5992.
14 N. J. Knight, E. Hernando, C. J. E. Haynes, N. Busschaert, H. J. Clarke, K. Takimoto, M. García-Valverde, J. G. Frey, R. Quesada and P. A. Gale, *Chem. Sci.*, 2016, **7**, 1600–1608.
15 I. Carreira-Barral, M. Mielczarek, D. Alonso-Carrillo, V. Capurro, V. Soto-Cerrato, R. Pérez Tomás, E. Caci, M. García-Valverde and R. Quesada, *Chem. Commun.*, 2020, **56**, 3218–3221.
16 P. A. Gale, C. C. Tong, C. J. E. Haynes, O. Adeosun, D. E. Gross, E. Karnas, E. M. Sedenberg, R. Quesada and J. L. Sessler, *J. Am. Chem. Soc.*, 2010, **132**, 3240–3241.
17 D. S. Kim and J. L. Sessler, *Chem. Soc. Rev.*, 2015, **44**, 532–546.
18 P. A. Gale, M. E. Light, B. McNally, K. Navakhun, K. E. Sliwinski and B. D. Smith, *Chem. Commun.*, 2005, 3773–3775.
19 N. J. Roy, P. L. Pujari and P. Talukdar, *Org. Biomol. Chem.*, 2023, **21**, 3323–3329.
20 F. G. Bordwell, G. E. Drucker and H. E. Fried, *J. Org. Chem.*, 1981, **46**, 632–635.
21 N. M. Koropatkin, H. B. Pakrasi and T. J. Smith, *Proc. Natl. Acad. Sci. U. S. A.*, 2006, **103**, 9820–9825.
22 J. J. He and F. A. Quiocho, *Science*, 1991, **251**, 1479–1481.
23 N. M. Koropatkin, D. W. Koppenaal, H. B. Pakrasi and T. J. Smith, *J. Biol. Chem.*, 2007, **282**, 2606–2614.
24 K. H. G. Verschueren, F. Seljée, H. J. Rozeboom, K. H. Kalk and B. W. Dijkstra, *Nature*, 1993, **363**, 693–698.
25 K. J. Chang, D. Moon, M. S. Lah and K. S. Jeong, *Angew. Chem., Int. Ed.*, 2005, **44**, 7926–7929.
26 P. A. Gale, *Chem. Commun.*, 2008, 4525–4540.
27 P. A. Gale, J. R. Hiscock, C. Z. Jie, M. B. Hursthouse and M. E. Light, *Chem. Sci.*, 2010, **1**, 215–220.
28 C. Caltagirone, P. A. Gale, J. R. Hiscock, M. B. Hursthouse, M. E. Light and G. J. Tizzard, *Supramol. Chem.*, 2009, **21**, 125–130.
29 G. W. Bates, Triyanti, M. E. Light, M. Albrecht and P. A. Gale, *J. Org. Chem.*, 2007, **72**, 8921–8927.
30 S. J. Moore, M. Wenzel, M. E. Light, R. Morley, S. J. Bradberry, P. Gómez-Iglesias, V. Soto-Cerrato, R. Pérez-Tomás and P. A. Gale, *Chem. Sci.*, 2012, **3**, 2501–2509.
31 L. A. Jowett, E. N. W. Howe, V. Soto-Cerrato, W. Van Rossom, R. Pérez-Tomás and P. A. Gale, *Sci. Rep.*, 2017, **7**, 9397.
32 S. B. Salunke, J. A. Malla and P. Talukdar, *Angew. Chem., Int. Ed.*, 2019, **58**, 5354–5358.
33 ChemAxon, 5.8.0 Marvin, (**https://chemaxon.com**), 2012.
34 L. Xiong, X. L. Zhu, H. W. Gao, Y. Fu, S. Q. Hu, L. N. Jiang, W. C. Yang and G. F. Yang, *J. Agric. Food Chem.*, 2016, **64**, 4830–4837.
35 D. Bastos-González, L. Pérez-Fuentes, C. Drummond and J. Faraudo, *Curr. Opin. Colloid Interface Sci.*, 2016, **23**, 19–28.
36 X. Wu and P. A. Gale, *Chem. Commun.*, 2021, **57**, 3979–3982.
37 A. Kerckhoffs and M. J. Langton, *Chem. Sci.*, 2020, **11**, 6325–6331.
38 R. L. Biltonen and D. Lichtenberg, *Chem. Phys. Lipids*, 1993, **64**, 129–142.
39 H. Goto and E. Osawa, *J. Am. Chem. Soc.*, 1989, **111**, 8950–8951.
40 H. Goto, S. Obata, N. Nakayama and K. Ohta, *CONFLEX* 8, CONFLEX Corporation, Tokyo, Japan, 2017.
41 M. J. Frisch, G. W. Trucks, H. B. Schlegel, G. E. Scuseria, M. A. Robb, J. R. Cheeseman, G. Scalmani, V. Barone, B. Mennucci, G. A. Petersson, H. Nakatsuji, M. Caricato, X. Li, H. P. Hratchian, A. F. Izmaylov, J. Bloino, G. Zheng, J. L. Sonnenberg, M. Hada, M. Ehara, K. Toyota, R. Fukuda, J. Hasegawa, M. Ishida, T. Nakajima, Y. Honda, O. Kitao, H. Nakai, T. Vreven, J. J. A. Montgomery, J. E. Peralta, F. Ogliaro, M. Bearpark, J. J. Heyd, E. Brothers, K. N. Kudin, V. N. Staroverov, T. Keith, R. Kobayashi, J. Normand, K. Raghavachari, A. Rendell, J. C. Burant, S. S. Iyengar, J. Tomasi, M. Cossi, N. Rega, J. M. Millam, M. Klene, J. E. Knox, J. B. Cross, V. Bakken, C. Adamo, J. Jaramillo, R. Gomperts, R. E. Stratmann, O. Yazyev, A. J. Austin, R. Cammi, C. Pomelli, J. W. Ochterski, R. L. Martin, K. Morokuma, V. G. Zakrzewski, G. A. Voth, P. Salvador, J. J. Dannenberg, S. Dapprich, A. D. Daniels, O. Farkas, J. B. Foresman, J. V. Ortiz, J. Cioslowski and D. J. Fox, *Gaussian 09, Revision D.01*, Gaussian, Inc., Wallingford CT, 2013.
42 A. D. Becke, *J. Chem. Phys.*, 1993, **98**, 5648–5652.
43 C. Lee, W. Yang and R. G. Parr, *Phys. Rev. B: Condens. Matter Mater. Phys.*, 1988, **37**, 785.
44 P. C. Hariharan and J. A. Pople, *Theor. Chim. Acta*, 1973, **28**, 213–222.
45 M. M. Francl, W. J. Pietro, W. J. Hehre, J. S. Binkley, M. S. Gordon, D. J. DeFrees and J. A. Pople, *J. Chem. Phys.*, 1982, **77**, 3654–3665.
46 *BindFit, v0.5*, **https://app.supramolecular.org/bindfit/**.
47 M. Tsukimoto, H. Harada, A. Ikari and K. Takagi, *J. Biol. Chem.*, 2005, **280**, 2653–2658.